17.7 PREDICTING PROPAGATING CONVECTIVE SYSTEMS USING OPERATIONAL FORECAST MODELS

Melissa S. Bukovsky*
University of Oklahoma, Norman, OK

John S. Kain
CIMMS/University of Oklahoma/NSSL, Norman, OK

1. INTRODUCTION

Over the United States, most significant precipitation-producing events (24h amounts ≥ 0.50 in.) occur during the warm season (Olson et al. 1995). Unfortunately, during the time of the year when the rainfall is heaviest, skill scores for quantitative precipitation forecasts (QPFs) are relatively low (Charba and Klein 1980; Olson et al. 1995). This may be attributed ultimately to the main differences between many warm and cool season precipitation events. Specifically, warm season precipitation is not usually the stable, gradually developing, relatively expansive type seen in the cool season and is often associated with smaller scale atmospheric processes (e.g., Houze and Hobbs 1982). In fact, Heideman and Fritsch (1988) concluded that over 80% of the rainfall in significant warm-season events is associated with deep convection, or thunderstorms.

In theory, thunderstorms have inherent predictability limitations (Lorenz 1969; Lilly 1990). Yet, convection is often associated with larger scale disturbances that have much longer predictability time scales. For instance, much of the heavy rain produced during the warm season falls from mesoscale convective systems (MCSs) (Fritsch et al. 1986), many of which initiate in association with larger scale dynamic disturbances. Even when such a precursor is apparently absent, mid-latitude summertime rainfall patterns can be coherent on time scales considerably longer than the lifetime of individual MCSs, suggesting that an even higher level of predictability exists, at least for some convective systems (Carbone et al. 2002). It would appear, therefore, that the intrinsic limitations on predictability are not the central cause for the low warm-season precipitation forecasting skill.

It has been shown that the skill of forecasters in predicting significant precipitation events is directly related to the skill of the numerical models that they use (Olson et al. 1995; Fritsch et al. 1998). Thus, the relatively poor performance of operational forecast models during the warm season is likely an important limiting factor in accurately predicting heavy rainfall events (Mesinger 1996; Corfidi 2003). Current operational models are incapable of resolving deep convection; thus, introducing a model-forecast contingency to convective parameterization. This has been blamed for the fundamental initiation and propagation errors found in simulations of warm-season rainfall and, consequently, the poor forecasts of these events over the United States (Davis et al. 2003). Whether convection is parameterized or not, correct forecasts require that convective systems are initiated at the right time and place and that they move in the right direction. In other words, forecast models must represent the operative processes involved in convective initiation and propagation. A review of some of the processes involved in propagation follows.

1.1 Propagation

Mesoscale convective systems display many different modes and configurations of mesoscale organization, as shown in Houze et al. (1990). The clustered or linear organization of many systems appears to be related to the collective effect of multiple downdraft outflow circulations. However, as Mapes (1993) points out, this conglomeration also occurs naturally as activated clouds alter the local environment by inducing wavelike pulses that can trigger further development close to existing cells.

Either organizing mechanism can also contribute to the propagation of MCSs away from a truly advective motion. For an MCS to exhibit a speed and direction of motion that is not directly linked to some steering level or external forcing in the atmosphere, it must generate convective scale feedbacks that induce upscale growth and produce a mesoscale response. While individual cells may move advectively, system movement is determined by the triggering of new cells. Cells may be triggered by a mesoscale or larger-scale disturbance that is moving slower than the advective flow or by circulations invoked by upscale growth mechanisms, allowing the system as a whole to move in a manner that is not advective. In the absence of large scale, dynamic forcing, furthermore, propagation can provide means for continued growth into regions where it would not be otherwise favored (Carbone et al. 2002). A brief review of some of the explanatory theory follows.

1.1.1 *Cold pools and gust fronts*

One of the more easily observed features of propagating MCSs is the cold pool. Cold pools form behind or below a leading convective line as convective downdrafts deposit air that has been cooled by sublimation, melting, and/or evaporation of precipitation. The boundary marked by low-level outflow convergence and ascent at the edge of a cold pool, or the gust front, is often associated with new cell development. Moreover, development is favored where low-level

* *Corresponding author address:* Melissa S. Bukovsky, NSSL, 1313 Halley Circle, Norman, OK, 73069; e-mail: melissa.bukovsky@noaa.gov

environmental inflow is greatest relative to gust front motion (Corfidi 2003). Successive formation of these new elements helps define the motion of a given MCS and, therefore, links cold pool motion to the propagation of the system.

In many cases, gust front motion can be likened to that of a density current (e.g. Charba 1974; Carbone et al. 1990; Stensrud and Fritsch 1993). Using this approximation, the speed of the gust front, V_c, is mostly dependant on the depth of the outflow, H, and the density difference between the warm air ahead of the gust front and the cold air behind it, as noted by the virtual temperatures T_{vw} and T_{vc}, respectively, in the following equation:

$$V_c = k\left(gH\frac{T_{vw}-T_{vc}}{T_{vc}}\right)^{1/2} + 0.62V_e\,, \qquad (1)$$

where k is the internal Froude number, g is the acceleration due to gravity, and V_e is the layer-averaged wind component parallel to the current motion over the depth H in the environment ahead of the gust front (Simpson and Britter 1980). For common cold pool environments, $\frac{T_{vw}-T_{vc}}{T_{vc}}$ is approximately 0.01 – 0.05. Neglecting the second term, setting k=1 (estimate of k in thunderstorm-induced density currents given in Bluestein (1993)), and allowing a depth of 1000m, plausible density current speeds vary between about 10-22 m/s.

1.1.2 *Gravity waves*

In theory, the relative motion of an internal gravity wave resembles that depicted by figure 1. Following Lindzen and Tung (1976), this type of wave travels with the phase speed:

$$C_{D,n} \approx \frac{NH}{\pi(1/2+n)}, n = 0,1,2,\ldots, \qquad (2)$$

where $C_{D,n}$ is the phase speed of mode n relative to the flow through the layer with depth H. N is the square root of the Brunt-Väisala frequency, which is defined as:

$$N^2 = \frac{-g}{\rho_0}\frac{\partial \rho_0}{\partial z}, \qquad (3)$$

where ρ_0 is the mean density of the surrounding atmosphere as a function of height. Waves will propagate horizontally outward from their source if properly ducted. For the conditions necessary for horizontal propagation without loss of energy or continual forcing see Lindzen and Tung (1976) and Crook (1988). If the wave is continually reinforced and is propagating with its forcing mechanism, ducting becomes less important since wave energy will not be traveling away from its source.

The gravity-wave-like response of the atmosphere to convective heating has been well studied (e.g. Emanuel 1983; Raymond 1987; Nicholls et al. 1991; Cram et al. 1992; Mapes 1993). When deep convection begins, it often induces a pulse-like response in the surrounding environment. However, as Mapes (1993) and, later, Pandya and Durran (1996) point out, it is somewhat misleading to identify this pulse as a gravity wave. The wave pulse, unlike a true linear gravity wave, *does* irreversibly modify the environment through which it passes.

In several of these studies, two modes corresponding to two simple heating structures were found to disperse most of the heating perturbations from convection. The first and most prominent mode dominates with an all-heating structure that corresponds well with the latent heating produced by the convective portion of an MCS (the n=0 mode Fig. 2a). It has a vertical wavelength that is twice the depth of the convective element. The second mode has a vertical wavelength equal to cloud depth and is most prominent with a heating aloft – cooling below profile that is similar to that produced by a region of stratiform precipitation (the n=1 mode in Fig. 2b). Superimposing these modes (Fig. 2c) to resemble a structure similar to the overall effect of leading line – trailing stratiform systems, and forcing it in a simple model yields, after a time, a gravity wave response dominated by a fast moving area of subsidence far away from its point of origin and a slower moving region of upper-level rising and low-level sinking motion behind it, associated with the n=0 and n=1 modes, respectively (Fig. 3); turning off the heating

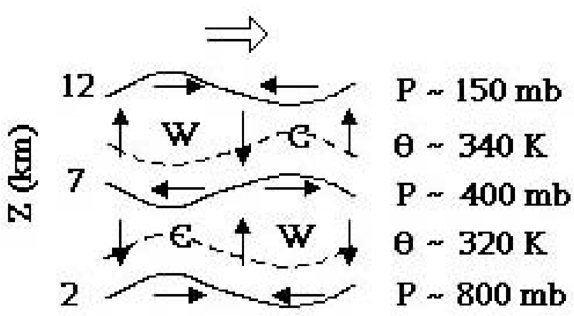

Fig. 1. Vertical cross section of the relative motion, pressure, and temperature perturbations in a propagating, linear internal gravity wave. The wave is propagating to the right. Arrows are drawn in the region of maximum relative velocity in that direction; C and W indicate areas of relative cooling and warming, respectively. The solid lines represent isobaric surfaces.

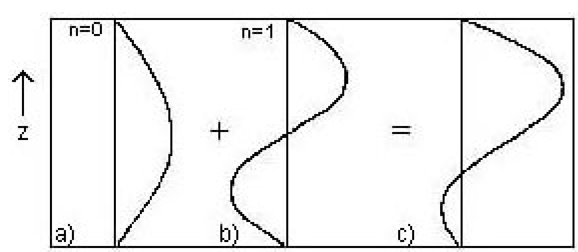

Fig. 2. Vertical distribution of thermal forcing. Straight vertical lines denote zero heating; left is negative, right is positive. (Adapted from Nicholls et al. (1991) Fig. 4)

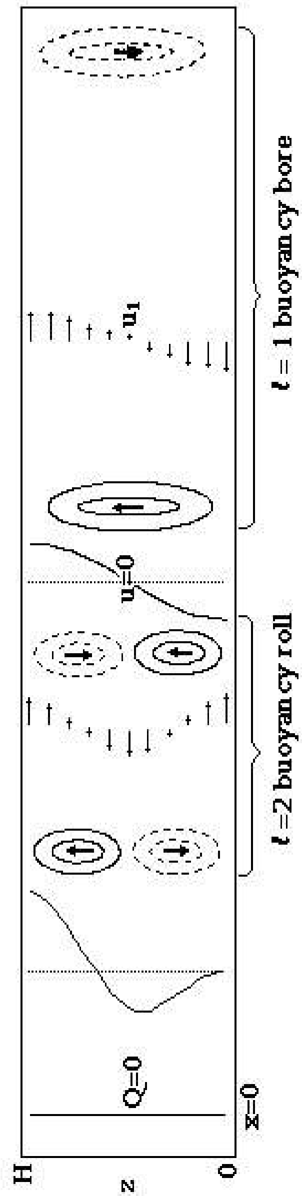

Fig. 3. (Fig. 6 from Mapes (1993)) Schematic of buoyancy bores, horizontal winds, and horizontal displacements of material lines after a given time for the heating profile used in Mapes (1993). The heating profile that initiated these bores is somewhat similar to those imposed in this study. A two mode heat source was forced near x = 0. Heating was then turned off after a given amount of time, yielding rolls in the opposite sense. ℓ = 1 corresponds to mode n = 0, and ℓ = 2 corresponds to mode n = 1 in this study.

yields the reverse response.

These modes are important because motions caused by them may play a role in the organization and propagation of convection. The second mode causes boundary layer convergence as it passes, favoring additional convection (Mapes 1993). A sort of gravity wave – convective line constructive interference may also occur when the convection and the second mode are coupled and travel together (Raymond 1983, 1987; Xu and Clark 1984; Cram et al. 1992). Many of the studies on this subject, though, are based on theory and/or have been done in 2-D environments, most of which are quite quiescent to start. In a later section, an attempt will be made to identify similar features in a 3-D environment that is full of the atmosphere's standard disturbances.

1.2 Initiation and Propagation of Convection within Convective Parameterization Schemes

It is the goal of convective parameterization to communicate the effects of sub-grid scale clouds using resolved scale variables. In order for processes involved in initiation to be successfully included in this formulation, therefore, they must usually be of a resolvable scale[*].

The first link between convection and the resolvable scale occurs when the decision is made by some "trigger function" to allow convection at a grid point. Trigger functions come in many formulations for many different grid resolutions and, as illustrated by studies conducted by Kain and Fritsch (1992), Stensrud and Fritsch (1994), Chaboureau et al. (2003), and Jakob and Siebesma (2003), they can have a great impact on the representation of convection within a numerical model.

As for the propagation of MCSs in numerical models, convective parameterizations have not been specifically designed to handle this process. Propagation within a model utilizing a convective parameterization scheme (CPS) is dependent upon the upscale growth of convective effects such that a mesoscale response is induced on the resolved scales. Without the generation of a substantial mesoscale circulation, precipitation features covering a mesoscale area will behave like a collection of isolated entities, since a parameterization acts independently in individual model columns (Kain and Fritsch 1998). The lack of propagation in warm season rainfall in short range NWP models due to convective parameterizations has been documented by Carbone et al. (2002), Davis et al. (2003), and Moncrieff and Liu (2003).

1.3 Objectives

In this study a popular CPS will be used to examine the extent to which convective feedbacks lead to the propagation of a simulated MCS. The Betts-Miller-Janjić scheme (Betts 1986; Betts and Miller 1986; Janjić 1994; hereafter BMJ) will be used in this study since it has been used for years by forecasters and research scientists at the National Center for Environmental Prediction's (NCEP's) Storm Prediction

[*] A caveat is implied here since some parameterizations utilize sub-grid scale quantities. For instance, some shallow cloud parameterizations make use of turbulence statistics from planetary boundary layer schemes (see Deng et al. 2003, Neggers et al. 2004), and in various applications of the convective parameterization proposed by Arakawa and Shubert (1974), surface flux tendencies are included in the calculation of the cloud work function.

Center (SPC) and the National Severe Storms Laboratory (NSSL) (Kain et al. 2001). Peculiarities in the Eta with the BMJ CPS (Eta-BMJ) in the prediction of organized MCSs have been noted by the previously mentioned users. However, it is still not entirely understood how this type of convective event is being handled in the model with this convective scheme, providing motivation for this study. The treatment of propagation by the BMJ scheme will, therefore, be investigated. The model formulations used to do so will be presented in the next section. A case study will be presented in section 3, and the mechanisms responsible for propagation will be examined in section 4. To conclude, a discussion of the results will be presented in section 5.

2. MODEL FRAMEWORK

The Eta model (Black 1994) was used for this study. The configuration used is identical to the 22-km, 50 layer version of the model used operationally from September 2000 through November 2001, except that all integrations were made over a slightly smaller domain than that which is used operationally, fourth-order nonlinear horizontal diffusion was applied to each

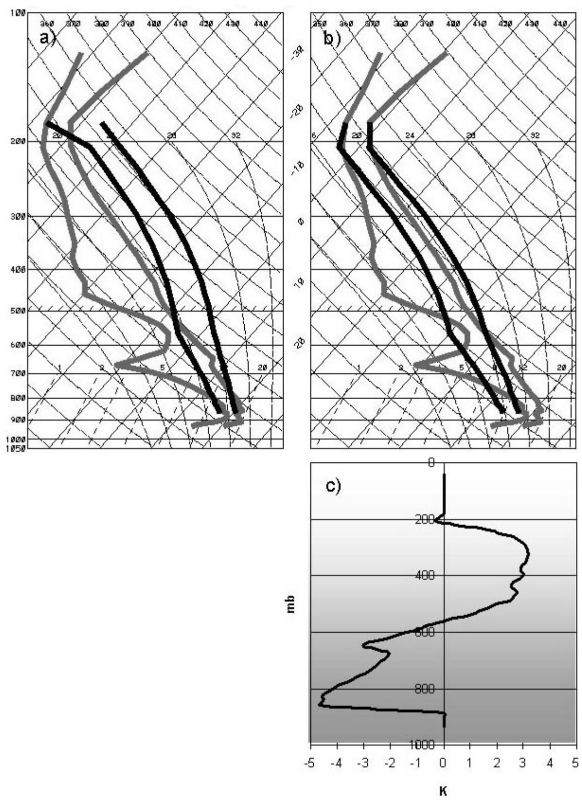

Fig. 4. Convective adjustment using the BMJ scheme for a point in northeast South Dakota around 1000 UTC in the Eta-BMJ run.
a, b) Initial environment temperature and dewpoint temperature shown in dark grey. a) First-guess adjustment profiles in black. b) Final adjustment profiles in black. c) Temperature difference between initial and final environments.

of the principal variables after each adjustment time step (as opposed to the operational second-order diffusion), and the convective parameterization was applied at every model time step.

2.1 The BMJ Deep Convection Scheme

The BMJ scheme is a convective adjustment type scheme. It applies a lagged adjustment towards predetermined reference profiles of temperature and dewpoint, approximating convective equilibrium. To begin, the scheme finds the most unstable model parcel within roughly 200 hPa of the surface and calculates cloud properties from this parcel. If cloud depth is sufficient, additional criteria are evaluated to assess the potential for activation of deep convective feedbacks.

First, reference profiles for temperature, $T_R(K)$, and water vapor, $q_R(kg\ kg^{-1})$, are calculated. These profiles always exhibit a shape similar to that shown in figure 4a. The reference, or first-guess, temperature profile is fixed at cloud base at the original temperature and then diverges from the moist-adiabat used to define the cloud with a slightly higher lapse rate with height until the freezing level is reached. Above this level, the temperature profile converges back toward moist-adiabatic as it approaches cloud top. The corresponding profile for q_R is calculated such that dewpoint depressions of about 3-5°C exist at cloud base and cloud top with a depression of 7-9°C at the freezing level (Baldwin et al. 2002).

The first-guess reference profiles are then compared to the original model values for T and q and adjusted/shifted as a pair (without changing their position relative to one another) until latent heat release due to convection is balanced by the removal of water vapor through the depth of the convective layer. As applied to the sounding in figure 4a, the correction process would shift the first-guess profiles to the left. This shift would produce the final adjusted profiles seen in figure (Fig. 4b). Note that during this process, the separation between the temperature and specific humidity reference profiles remains constant.

Given the imposed separation between T_R and q_R, the final correction process results in net cooling and moistening when the column is relatively dry. When this happens in the scheme, deep convection is not allowed. Because net heating and drying must occur (the generation of precipitation requires the net removal of moisture and latent heat release), layers that are warm and/or dry initially tend to inhibit convection. Thus, deep-layer moisture convergence and convective inhibition implicitly modulate deep convective activity within the BMJ scheme, even though these factors are not considered explicitly (Baldwin et al. 2002).

3. CASE STUDY

The event chosen for this study occurred from 11-12 June 2001. On these dates, a large complex of thunderstorms moved through Minnesota and Wisconsin into parts of Illinois, Indiana, and Ohio.

3.1 Observations

Severe thunderstorms formed on the afternoon of 11 June 2001 around 1800 UTC in west-central Minnesota and southeastern North Dakota. This complex of supercellular, tornado producing storms occurred along and just north of a warm front that extended eastward from a surface low positioned over south-west Minnesota and eastern South Dakota (Fig. 5a; see Fig. 6 for a radar depiction of the storms). Storms also were formed along a cold front that extended southward and south-westward from the surface low, but these storms were relatively weak and transient compared to the activity north of the warm front.

A 15 – 20 m/s 850-hPa jet extending from the southern plains into Iowa and southern Minnesota brought unstable air into this region (Fig. 5c), while strong upper-level flow with imbedded short-waves induced synoptic scale lift in this region (Fig. 5b). The environment was quite unstable and deep layer wind shear was also significant. For example, the 1800 UTC 11 June 2001 sounding from Chanhaussen, MN (MPX) revealed a mid-level (700-500 hPa) lapse rate of 8.6°C/km, a CAPE value of 3342 J/kg (most unstable parcel in the lowest 300mb), and a surface to 6-km shear value of 28 m/s (Fig. 7). The surface conditions south of the front were warmer and moister, but also strongly capped, as 700-hPa temperatures hovered around 12°C in this part of Minnesota. These conditions moved eastward with the surface low as time progressed.

As evening approached, the storms propagated southeastward into Wisconsin (see figure 6 for the radar evolution of the MCS). While entering the central portion of the state, around 0000 UTC 12 June 2001, they began to organize into a more linear structure. Within a couple of hours, the system took on the form of a large, damaging-wind producing bow echo. Propagation took on an increasing southward component with time, and as the system neared Lake Michigan it showed evidence of a bookend vortex on the north-eastern end of the line for several hours.

Around 0600-0700 UTC on the 12th, after traversing much of Lake Michigan and parts of the bordering states and entering Indiana, the leading line began to weaken. Evidence of the complex still existed, though, into the morning hours of that day.

3.2 Eta Model Forecast

The model simulation of this event was initialized using 0000 UTC 11 June 2001 initial conditions. By 1800 UTC 11 June 2001, the model surface low is located in eastern South Dakota, quite close to its observed location (see figure 8a). Unfortunately, parameterized convection has already modified the model atmosphere at this time, making it difficult to compare other surface features to those observed around 1800 UTC. The warm front is clearly discernable at earlier times, but is distorted by the

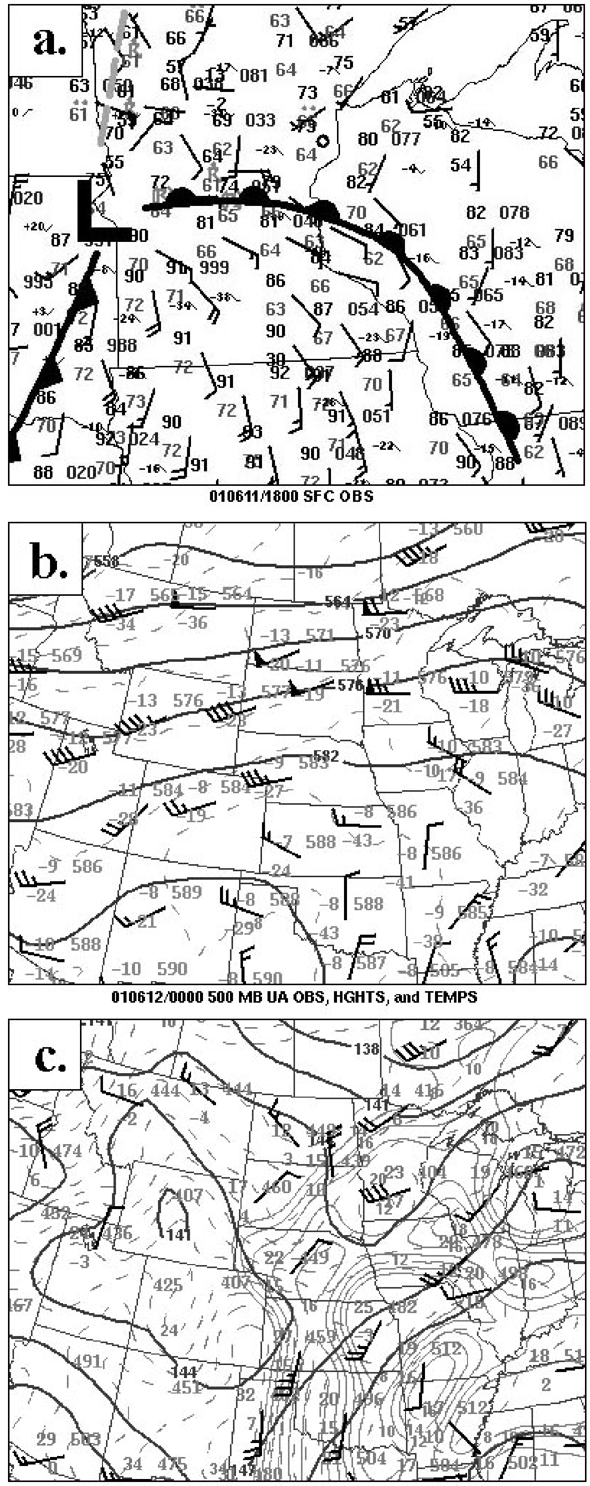

Fig. 5. a) Surface map from 1800 UTC 11 June 2001. b, c) Upper air maps from 0000 UTC 12 June 2001. b) 500 hPa observed winds, heights (contoured in heavy, dark grey lines), and temperatures (contoured in light grey, dashed lines). c) 850 hPa observed winds, heights (contoured in heavy, dark grey lines), temperatures (contoured in light grey, dashed lines), and dew point temperatures (contoured in light grey, solid lines).

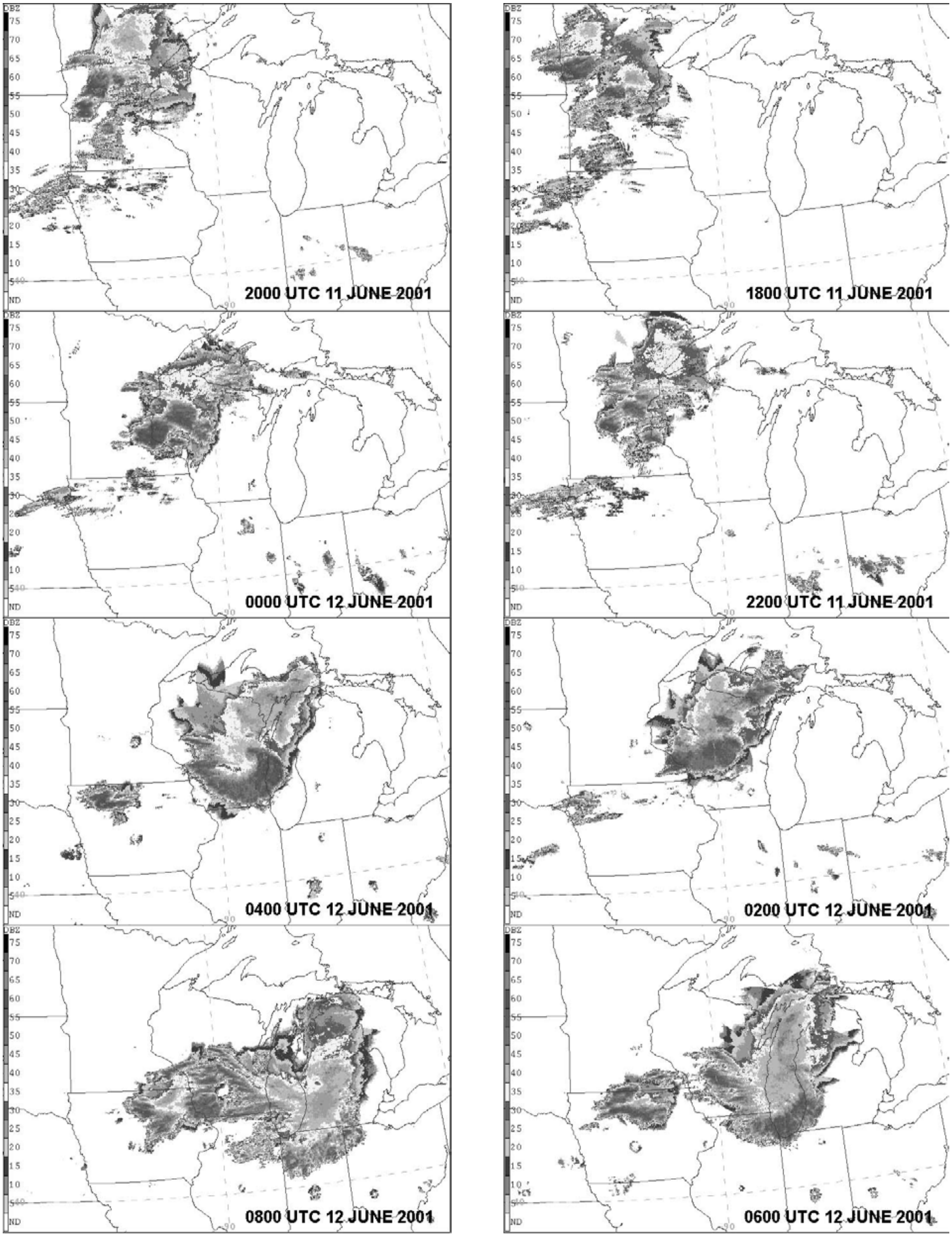

Fig. 6. 1 hourly composite base reflectivity displayed as the maximum reflectivity within the past hour at each pixel, shown every two hours from 1800 UTC 11 June 2001 to 0800 UTC 11 June 2001.

convective cooling effects at 1800 UTC. Realistic upper level features are also visible in the model (compare Fig. 8 b, c and Fig. 5 b, c). Furthermore, the magnitude of the instability over the region is captured in the model, as evidenced by CAPE values up to ~5000 J/kg ahead of the precipitation area (not shown).

The precipitation produced in this run is shown in figure 9. As illustrated, the Eta-BMJ, is able to initiate parameterized convection, expand it to cover a mesoscale area, develop a bow-shaped convective system, and propagate this system to the right of the mid-level steering currents; evolving it quite similarly to observations. As mentioned, though, the timing of the complex is off. The model run develops the system upstream from its observed location, several hours ahead of time, and the southward propagation component is too strong, carrying the precipitation area into Iowa at about 18 m/s instead of into Indiana. Nonetheless, it is intriguing that the Eta-BMJ run created a convective system with a distinctive and realistic mesoscale evolution in this environment. In examining just how this feature develops and propagates, perhaps we can identify important clues about how parameterized convection can induce a strongly propagating system.

4. REVEALING THE OPERATIVE MECHANISMS FOR THE DIFFERENT BEHAVIORS

Specific characteristics of the environment and the convective parameterization allow propagation to occur on this day in the model forecast. On 11 June 2001, strong mid-level lapse rates are present coupled with more stable air towards cloud base. This allows the BMJ adjustment process to produce very distinctive convective tendencies. As shown in figure 4, the BMJ adjustment process produces a temperature profile that bisects this particular environmental profile in such a

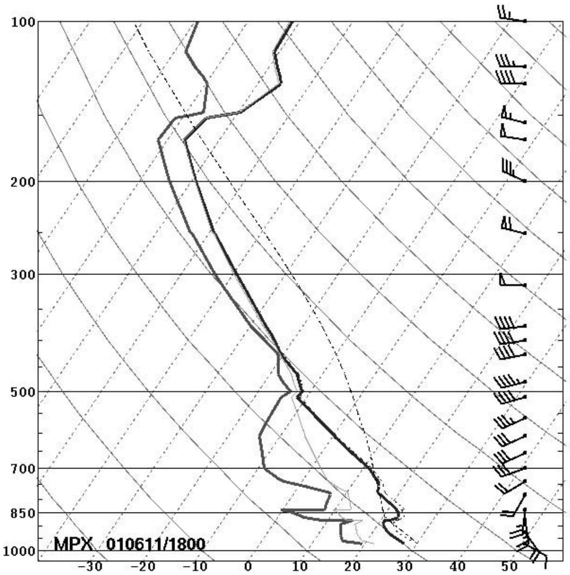

Fig. 7. 1800 UTC 11 June 2001 sounding from Chanhaussen, MN (MPX).

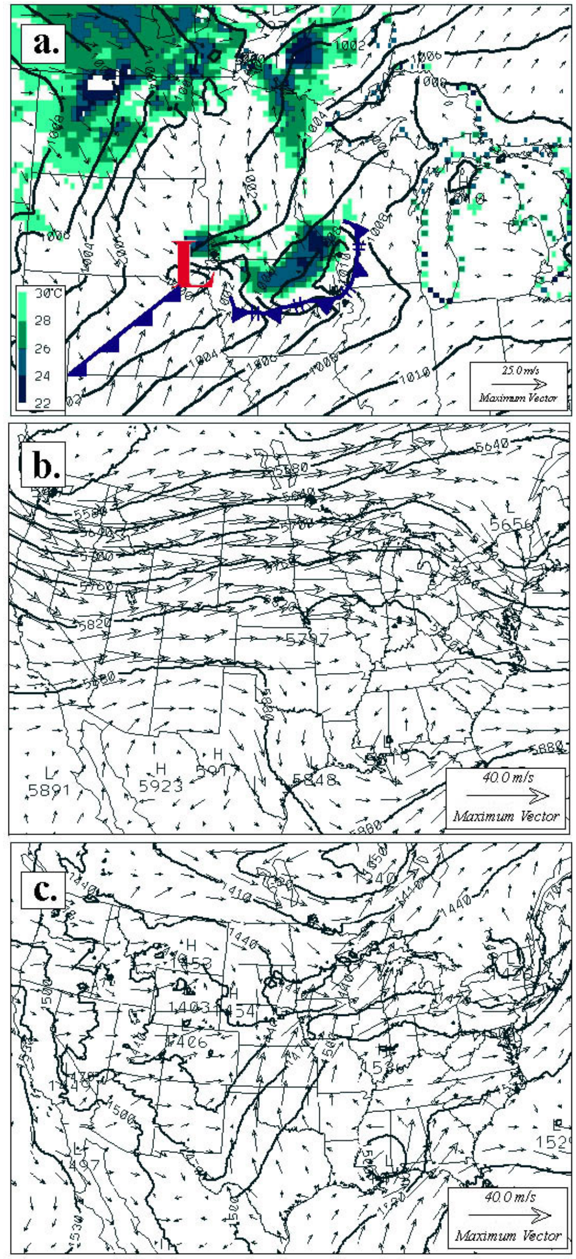

Fig. 8. Model forecasts from the Eta-BMJ.
a) **Surface** forecast for *1800 UTC 11 June 2001*. Isobars analyzed every 2 hPa (heavy black lines). Surface temperature shaded from 22 – 30 °C. Surface features analyzed following Young and Fritsch (1989).
b) **500-hPa** model forecast for *0000 UTC 12 June 2001*. Height contours every 60 gpm.
c) **850-hPa** model forecast for *0000 UTC 12 June 2001*. Height contours every 30 gpm.

way that strong negative tendencies are produced in the lowest portion of the cloud layer with positive tendencies aloft (Fig. 4c). The impact of this heating distribution is clearly visible in figure 10b, which shows that the forward edge of the convective region experiences sharp cooling in the lower half of the cloud layer and warming aloft. These temperature anomalies produce a local hydrostatic imbalance that induces subsidence in the lower half of the troposphere and upward motion aloft. This response produces adiabatic warming (lower half) and cooling (aloft), reversing the anomalies created by the parameterized convective tendencies and producing the four-cell look of the temperature-change field when viewed as a cross section through the convective line (Fig. 10b). Note, also, that the near surface cooling that lies just behind the leading edge of the convection present in the model forecast in figure 10b is not a direct result of the convective tendencies. BMJ-type convective feedbacks do not directly modify the environment below cloud base. Instead, this cold pool like feature is created through turbulent mixing of the superadiabatic layer left at cloud base after BMJ type convective feedbacks have been imposed (Fig. 11).

As discussed in the introduction, convective systems must induce propagation through internal forcing in order to move in a manner that is not determined purely by larger-scale forcing mechanisms. In this case, it would appear that the convective feedbacks in this run are doing just that. The existence (or absence) of two common propagation forcing mechanisms in these simulations will be explored in the following sections.

4.1 The Role of Gravity Waves

The appearance of the bowing convective complex in the simulation suggests that the system propagates in a manner similar to a solitary internal gravity wave.

To start, notice that the convective heating profile in figure 4c resembles the profiles seen in figures 2b and 2c. The cross section in figure 10 also depicts motions and temperature trends that are similar to those derived from theory (Fig. 1). Among the most important of these similarities is the quarter-wavelength phase lag between the maximum vertical motions and the maximum temperature changes.

The propagation speed of the convective arc also suggests internal gravity wave motion. Precipitation in the simulation travels at 15-22 m/s depending on the time and the location within the system. This is fairly consistent with the calculated speed of an n=1 mode gravity wave in this environment. Using (2) and substituting H equal to cloud depth and N for this layer, the relative gravity wave phase speed for the simulation is approximately 17-18 m/s.

Propagation of gravity waves is possible because the upstream environment is stably stratified (not shown). Existing sharp gradients in the Brunt-Väisälä frequency at the tropopause and near cloud base are also conducive to the trapping of waves in the vertical. In this study, however, the wave propagates with its forcing mechanism (parameterized convection), never away from it. Therefore, while ducting of the

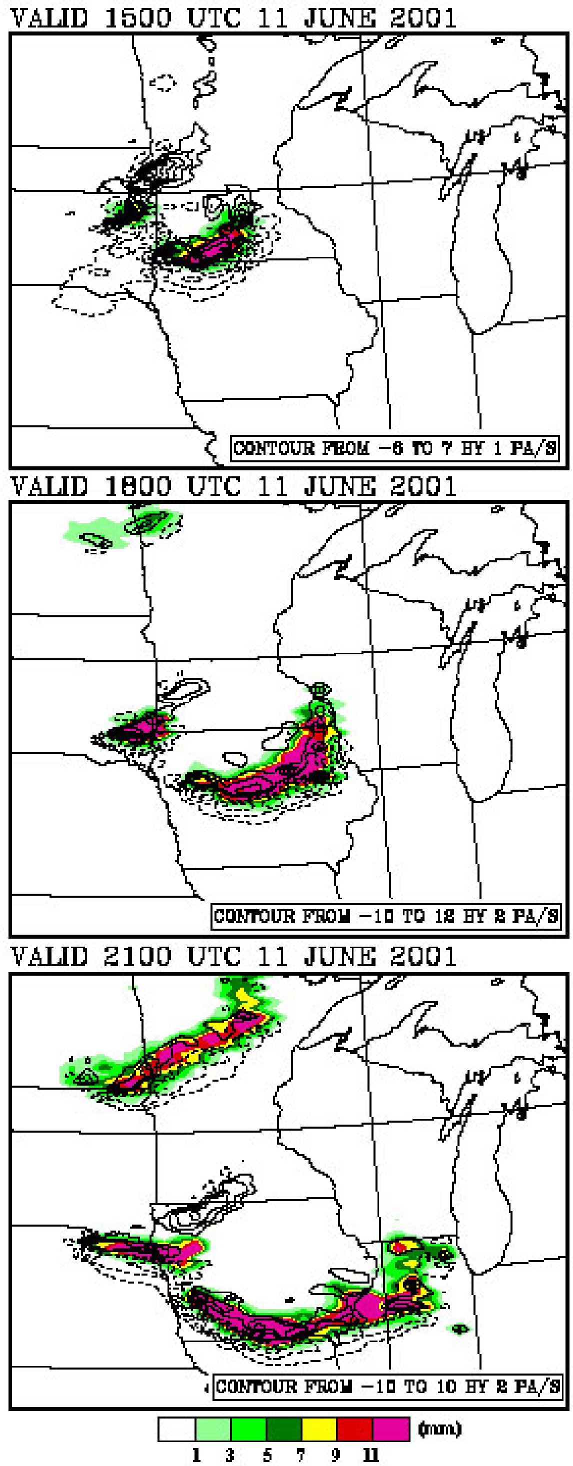

Fig. 9. One hour total precipitation accumulation at the surface (kg/m^2 = mm) and 700-hPa pressure vertical velocity (dashed lines indicate negative values, solid lines indicate positive values) from the Eta-BMJ run.

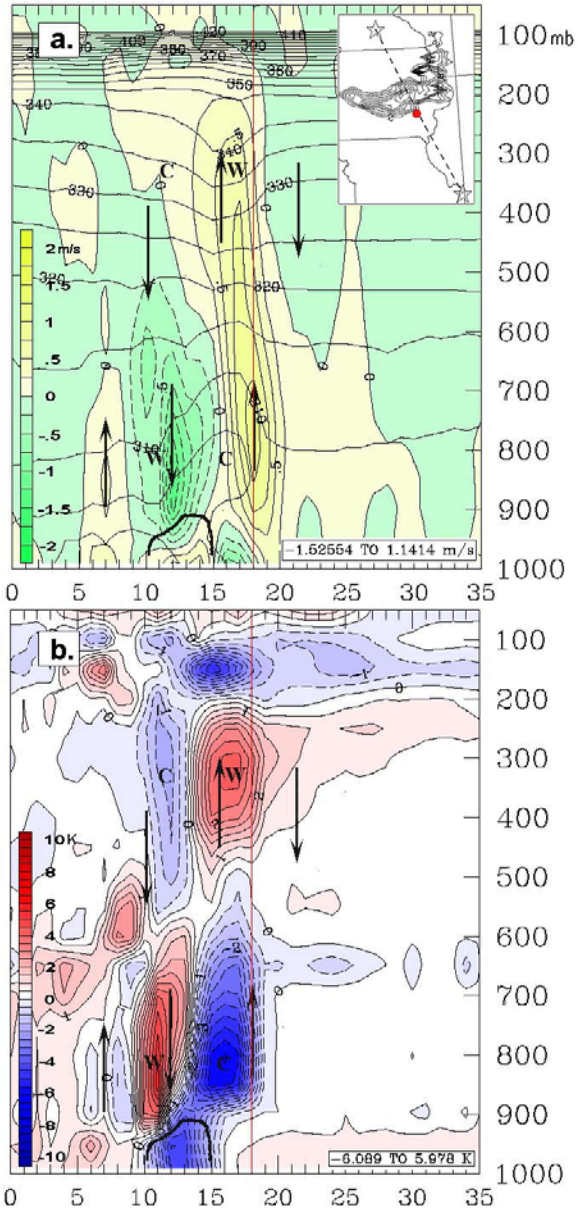

Fig. 10. Vertical cross sections from the Eta-BMJ run of: a) vertical velocity (contour interval of 0.2 m/s, negative values dashed) and potential temperature (K); b) 1-h temperature change (contour interval of 0.5 K, negative values dashed) for 1900 UTC 11 June 2001. Cross section location inset above. W and C indicate areas of warming and cooling, and vertical arrows represent vertical motions. The thick lower contour outlines the area of strong low level cooling. Horizontal axis for reference only. Distance between endpoints is about 433 km; each horizontal unit equals ~12 km. The vertical line at point 18 corresponds to the large centered dot on the cross section location image.

wave energy would certainly reduce dissipation, the more important factor in the longevity of the wavelike structure appears to be nearly continuous reinforcement from the convective scheme.

In this simulation, the wave-like feature arises as a response to the first instance of parameterized convection. As the convective scheme cools the lower half of the cloud layer and warms the upper half, it generates a hydrostatic imbalance that induces mid-level convergence, subsidence below, and upward motion aloft. This disturbance triggers a gravity-wave-like pulse with the mirror-image vertical motion profile – upward motion in the lower troposphere and subsidence aloft. The pulse radiates horizontally in an isotropic manner from the initial convective point; thus, allowing the lower level upward motion associated with it to further condition the atmosphere for convection in all directions. The extra cooling and moistening seems to allow the BMJ scheme to trigger at points that may not otherwise convect, and the points that do convect then feed more energy to the wave. This process seems responsible for the non-advective propagation component in this run.

The downward phase of the wave behind the lower-cloud-layer parameterized cooling is an adjustment response. Here, the model produces subsidence to warm the environment and counteract the convective cooling. Again, the opposite occurs in the upper portion of the cloud layer.

Once the convective system matures, the gravity wave-like feature becomes a constant, visible feature associated with the propagation of the convection in this case. Figure 12 illustrates this process during the mature stage of the bowing convective system in the Eta-BMJ run for the indicated point. In this time series, upward motion associated with the leading edge of the wave clearly precedes deep convection (indicated by the spike in the convective cooling tendency). Once convection occurs, the model responds by inducing subsidence, thus creating a wave-like structure in the vertical motion field at this level.

As mentioned earlier, the BMJ scheme was applied at every time step. In doing this, however, the convective tendencies in this Eta run were inadvertently multiplied by a factor of six. These stronger tendencies allowed the gravity wave feature to be quite obvious and, therefore, to be serendipitously identified. This error was later corrected, and similar results were found. The wave was still present, and the system produced in this run still propagated in a similar manner at a speed matching that of the gravity wave. Throughout this preprint, however, the run with the stronger tendencies was used for clarity, as the wave-like feature is not as clearly discernible in the cross sections from the run with the corrected tendencies.

4.2 The Role of Cold Pools

As mentioned above, cold pool like features are created in the Eta run through a turbulent mixing process. Like the gravity wave element, the cold pools in these runs are also continually reinforced as indirect consequences of the convective feedbacks and, therefore, may play a role in the organization and propagation of the convective systems in question. As calculated using equation (1), the speed of a density

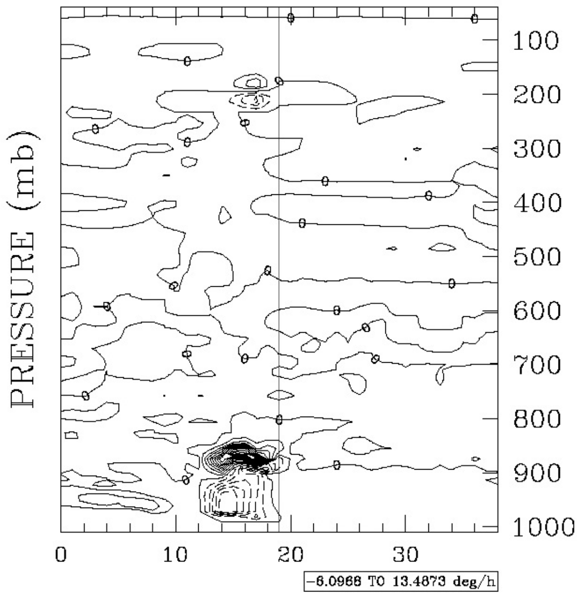

Fig. 11. Cross section of the turbulence temperature tendency in the Eta-BMJ for the same time and location as the cross sections in figure 21. Negative values are dashed.

current defined by the cold pool present at 19-h in the Eta would be roughly 8-9 m/s. Although a bit slow, this speed is still close to the noted propagation rate. The effect of the cold pool on propagation is, therefore, still difficult to separate from any other effect at this time.

5. DISCUSSION

What is intriguing about the forecast produced by the Eta on 11 June 2001 is that the BMJ scheme induces a realistic looking, strongly propagating, bowing convective line in an environment that actually supports such an evolution. Such predictions of convective propagation have significant potential value for both weather forecasting and climate simulations (Davis et al. 2003; Moncrieff and Liu 2003). Understanding the mechanisms of propagation is, therefore, of great interest.

Thus, in this study, the physical mechanisms of propagation important in the simulation of the 11 June 2001 MCS are identified and linked to specific characteristics of the environment and the convective parameterization. It was determined that a certain type of feedback from the BMJ convective scheme (strong cooling in the lowest portion of the cloud layer with warming aloft) induces gravity wave-like features that resonate with the parameterized convection, promoting propagation of the larger system. Strong upward motion associated with the forced gravity wave leads the convective systems and provides additional lift that favors new convection (refer back to Fig. 12 and the discussion at the end of section 4.1). The forced upward motion preconditions the atmosphere until it reaches a point where convection is able to occur. The time frame on this process is short enough for grid points to trigger sequentially and for system propagation to occur steadily because the environment is rather favorable to start.

Other methods of propagation were mentioned because, at this time, the effect of the cold pools in these runs has yet to be separated from the other features. Cold pools acting as density currents and internal gravity waves have, unfortunately, a common range of phase speeds in many environments, making it difficult to identify the dominant mechanism for MCS organization and evolution. More idealized simulations would be needed to determine cold pool effects versus the impact of the gravity wave features found in this case. It may be that the effect of the lagged downdrafts seen in the Eta run is similar to that seen in the theoretical work of Raymond (1987); where it was determined that the lagged downdrafts helped intensify the convective system and the forced gravity wave-like feature modulated the organization and propagation of the convection.

We can say now that propagation *does* occur in the Eta using the BMJ convective parameterization. This is quite significant because it is not the norm in models containing convective parameterizations. MCS life cycles are usually poorly represented because of the inability of convective feedbacks to undergo upscale growth and produce a mesoscale response on the grid scale, as mentioned in the introduction. Furthermore, even though the convective element simulated in this study propagated, allowing investigation of some of the possible mechanisms responsible for this phenomenon, it is still not known how to harness the features that are seemingly tied to it. Since understanding how to use these features and what other mechanisms come into play is important to the improvement of convective precipitation prediction for weather and climate, it is important that these issues be addressed in future work on this subject.

6. REFERENCES

Arakawa, A., and W. H. Schubert, 1974: Interaction of a

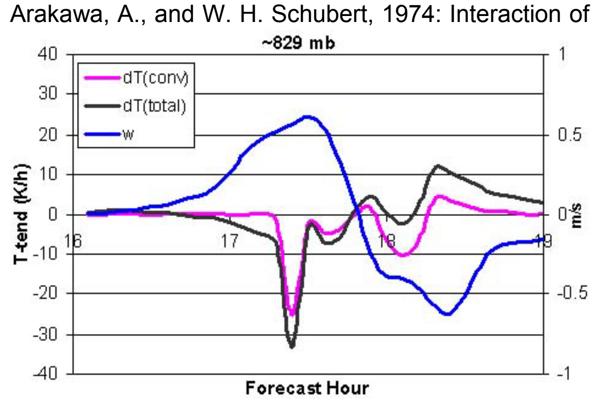

Fig. 12. Time series of vertical velocity (w, blue), the temperature tendency due to convection (dT(conv), magenta), and the total temperature tendency (dT(tot), black line) at about 829-hPa for a point in northwest Iowa in the Eta-BMJ run.

cumulus cloud ensemble with the large-scale environment, Part I. *J. Atmos. Sci.*, **31**, 674-701.

Baldwin, M. E., J. S. Kain, M. P. Kay, 2002: Properties of the convective scheme in NCEP's Eta model that affect forecast sounding interpretation. *Wea. Forecasting*, **47**, 1063-1079.

Betts, A.K., 1986: A new convective adjustment scheme. Part I: Observational and theoretical basis. *Quart. J. Roy. Meteor. Soc.*, **112**, 677-691.

___, and M. Miller, 1986: A new convective adjustment scheme. Part II: Single column tests using GATE wave, BOMBEX, and artic air-mass data sets. *Quart. J. Roy. Meteor. Soc.*, **112**, 692-709.

Black, T. L., 1994: The new NMC Eta model: Description and forecast examples. *Wea. Forecasting,* **9**, 265-278.

Bluestein, H. B., 1993: *Synoptic-Dynamic Meteorology in Midlatitudes.* Vol. 2, Oxford, 594 pp.

Carbone, R. E., J. W. Conway, N. A. Crook, and M. W. Moncrieff, 1990: The generation and propagation of a nocturnal squall line. Part I: Observations and implications for mesoscale predictability. *Mon. Wea. Rev.*, **118**, 26-49.

____, J. D. Tuttle, D. A. Ahijevych, and S. B. Trier, 2002: Inferences of predictability associated with warm season precipitation episodes. *J. Atmos. Sci.*, **59**, 2033-2056.

Chaboureau, J.-P., P. Bechtold, M. Köhler, A. Beljaars, M. Miller, J.-L. Redelsperger, 2003: Evaluation of cumulus parameterizations in simulating the diurnal cycle of convective precipitation over land. *Quart. J. Roy. Meteor. Soc.*, **128**, 1-18.

Charba, J. P., 1974: Application of gravity current model to analysis of squall-line gust front. *Mon. Wea. Rev.*, **102**, 140-156.

____, and W. H. Klein, 1980: Skill in precipitation forecasting in the National Weather Service. *Bull. Amer. Meteor. Soc.*, **61**, 1546-1555.

Corfidi, S. F., 2003: Cold pools and MCS propagation: Forecasting the motion of downwind-developing MCSs. *Wea. Forecasting*, **18**, 997-1017.

Cram, J.M., R.A. Pielke, and W.R. Cotton, 1992: Numerical simulations and analysis of a prefrontal squall line. Part II: Propagation of the squall line as an internal gravity wave. *J. Atmos. Sci.*, **49**, 209-225.

Crook, N.A., 1988: Trapping of low-level internal gravity waves. *J. Atmos. Sci.*, **45**, 1533-1541.

Davis, C. A., K. W. Manning, R. E. Carbone, S. B. Trier, and J. D. Tuttle, 2003: Coherence of warm-season continental rainfall in numerical weather prediction models. *Mon. Wea. Rev.*, **131**, 2667-2679.

Deng, A., N. L. Seaman, J. S. Kain, 2003: A shallow-convection parameterization for mesoscale models. Part I: Submodel description and preliminary applications. *J. Atmos. Sci.*, **60**, 34-55.

Emanuel, K. A., 1983: Elementary aspects of the interaction between cumulus convection and the large-scale environment. *Mesoscale Meteorology: Theories, Observations, and Models*, D. K. Lilly and T. Gal-Chen, Eds., D. Reidel, 551-575.

Fritsch, J. M., J. M., R. J. Kane, and C. R. Chelius, 1986: The contribution of mesoscale convective weather systems to the warm-season precipitation in the United States. *J. Climate Appl. Meteor.*, **25**, 1333-1345.

____, R. A. Houze Jr., R. Adler, H. Bluestein, L. Bosart, J. Brown, F. Carr, C. Davis, R. H. Johnson, N. Junker, Y.-H. Kuo, S. Rutledge, J. Smith, Z. Toth, J. W. Wilson, E. Zipser, and D. Zrnic, 1998: Quantitative Precipitation Forecasting: Report of the Eighth Prospectus Development Team, U.S. Weather Research Program. *Bull. Amer. Meteor. Soc.*, **79**, 285-299.

Heideman, K. F., and J. M. Fritsch, 1988: Forcing mechanisms and other characteristics of significant summertime precipitation. *Wea. Forecasting*, **3**, 115-130.

Houze, R. A., Jr., and P. V. Hobbs, 1982: Organization and structure of precipitating cloud systems. *Adv. Geophys.*, **24**, 225-315

____, B. F. Smull, and P. Dodge, 1990: Mesoscale organization of springtime rainstorms in Oklahoma. *Mon. Wea. Rev.*, **118**, 613-654.

Jakob, C., and A. P. Siebesma, 2003: A new subcloud model for mass-flux convection schemes: Influence on triggering, updraft properties, and model climate. *Mon. Wea. Rev.*, **131**, 2765-2778.

Janić, Z.I., 1994: The step-mountain eta coordinate model: Further developments of the convection, viscous sublayer, and turbulence closure schemes. *Mon. Wea. Rev.*, **122**, 927-945.

Kain, J. S., and J. M. Fritsch, 1992: The role of the convective "trigger function" in numerical forecasts of mesoscale convective systems. *Meteor. Atmos. Phys.*, **49**, 93-106.

____, and ____, 1998: Multiscale convective overturning in mesoscale convective systems: Reconciling observations, simulations, and theory. *Mon. Wea. Rev.*, **126**, 2254-2273.

____, M. E. Baldwin, P. R. Janish, S. J. Weiss, 2001: Utilizing the ETA model with two different convective parameterizations to predict convective initiation and evolution at the SPC. Preprints, *9th Conference on Mesoscale Processes*, Amer. Meteor. Soc., Ft. Lauderdale, FL, 91-95.

Lilly, D. K., 1990: Numerical prediction of thunderstorms – has its time come?. *Quart. J. Roy. Meteor. Soc.*, **116**, 779-798.

Lindzen, R.S., and K.K. Tung, 1976: Banded convective activity and ducted gravity waves. *Mon.Wea. Rev.*, **104**, 1602-1617.

Lorenz, E. N., 1969: Three approaches to atmospheric predictability. *Bull. Amer. Meteor. Soc.*, **50**, 346-349.

Mapes, B. E., 1993: Gregarious tropical convection. *J. Atmos. Sci.*, **50**, 2026-2037.

Mesinger, F., 1996: Improvements in quantitative precipitation forecasts with the Eta regional model at the National Centers for Environmental Prediction: The 48-km upgrade. *Bull. Amer. Meteor. Soc.*, **77**, 2637-2649.

Moncrieff, M. W., and C. Liu, 2003: Sequences of precipitation and organized convection: Dynamics and parameterization. *Symposium on Observing and Understanding the Variability of Water in Weather and Climate*, Long Beach, CA, Amer. Meteor. Soc., CD-ROM, 3.7.

Neggers, R. A., A. P. Siebesma, G. Lenderink, and A. A. M. Holstag, 2004: An evaluation of mass flux closures for diurnal cycles of shallow cumulus. Accepted for publication in *Mon. Wea. Rev.*

Nicholls, M.E., R.A. Pielke, and W.R. Cotton, 1991: Thermally forced gravity waves in an atmosphere at rest. *J. Atmos. Sci.*, **48**, 1869-1884.

Olson, D.A., N. W. Junker, and B. Korty, 1995: Evaluation of 33 years of quantitative precipitation forecasting at NMC. *Wea. Forecasting*, **5**, 570-575.

Pandya, R.E., and D.R. Durran, 1996: The influence of convectively generated thermal forcing on the mesoscale circulation around squall lines. *J. Atmos. Sci.*, **53**, 2924-2951.

Raymond, D. J., 1983: Wave-CISK in mass flux form. *J. Atmos. Sci.*, **40**, 2561-2572.

____, 1987: A forced gravity wave model of self-organizing convection. *J. Atmos. Sci.*, **44**, 3528-3543.

Simpson, J. E., and R. E. Britter, 1980: A laboratory model of an atmospheric mesofront. *Quart. J. Roy. Meteor. Soc.*, **106**, 485-500.

Stensrud, D. J., and J. M. Fritsch, 1993: Mesoscale convective systems in weakly forced large-scale environments. Part I: Observations. *Mon. Wea. Rev.*, **121**, 3326-3344.

____, and ____, 1994: Mesoscale convective systems in weakly forced large-scale environments. Part III: Numerical simulations and implications for operational forecasting. *Mon. Wea. Rev.*, **122**, 2084-2104.

Xu, Q., and J. H. E. Clark, 1984: Wave CISK and mesoscale convective systems. *J. Atmos. Sci.*, **41**, 2089-2107.